Dynamics and Radar Cross Section Density of Chaff Clouds

SHERMAN W. MARCUS
RAFAEL
Israel

A new chaff cloud model (CCM) is described which is based on fundamental principles with modifications based on laboratory observations. Excellent approximations to the exact physical model have been developed which can rapidly predict the chaff fiber density and orientation as a function of location, time and fiber characteristics. Using this information, the time varying radar cross section (RCS) density is determined for any frequency and polarization anywhere within the chaff cloud. The results are consistent with full scale observations, and the computational speed allows the model to be integrated into existing real time radar simulations.

Manuscript received October 1, 2002; revised July 25 and November 21, 2003; released for publication November 21, 2003.

IEEE Log No. T-AES/40/1/826457.

Refereeing of this contribution was handled by P. Lombardo.

Author's address: RAFAEL, EW Research and Simulation Center, PO Box 2250, Haifa 31021, Israel.

I. INTRODUCTION

Chaff is one of the simplest and most common measures employed to obfuscate the radar detection of aircraft targets. The determination of the radar cross section (RCS) of a chaff cloud can be divided roughly into 1) the aerodynamic solution which would define the cloud parameters as a function of space and time coordinates, and 2) the electromagnetic solution of scattering from this cloud. Aspects of these problems have been studied for many decades, particularly as applied to individual chaff fibers. Thus, the aerodynamic descent of a long and thin cylindrical particle in equilibrium can be described by a solution to Stokes equation [1], which assumes that the orientation of the fiber is known. Similarly, the RCS of the fiber can be determined by any of several methods [2, 3].

The application of these methods to a conglomerate of chaff fibers is far less common, in part because it would require knowledge of the orientation distribution of the fibers as a function of space and time. For the electromagnetic problem, many early studies assumed the equal likelihood of all fiber orientations. This assumption has since been ascertained to be overly simplistic, it now being recognized that wire-like fibers tend to fall with a horizontal or near horizontal orientation [4, 5]. As a result, more recent studies have assumed the equal likelihood of only the azimuth angles, while the elevation angle θ is taken to be statistically distributed about the horizontal [6]. Although this latter approach is more realistic, the use of such a distribution would aerodynamically affect the distribution of fiber orientations with altitude which would, in turn, affect the RCS distribution within the cloud.

In what follows, a new chaff cloud model (CCM) is described which utilizes fundamental aerodynamic principles to determine the density and orientation distributions of fibers within a chaff cloud, the RCS of which can then be determined. Section II describes the basic aerodynamic model, while Section III determines the corresponding fiber distribution in altitude for any given orientation distribution. The horizontal expansion predicted using this basic model is found to be lacking, but can be corrected by imposing a helical descent trajectory on each fiber in accordance with laboratory observations [7]. The mathematical model for accomplishing this is described in Section IV, and this leads to a horizontal fiber distribution that is detailed in Section V. This distribution is somewhat complex, but can be approximated using methods described in Section VI. The approximate horizontal fiber distribution is expressed in closed form in Section VII based on an assumed distribution of angular speeds of the fibers in the helical trajectories. In Section VIII, the fiber density is found as a function of radial location,

while in Section IX it is shown that, in accordance with observations [8], the model predicts a horizontal size beyond which the cloud will not expand. The fiber orientation distribution within the cloud and the RCS are determined in Section X. Finally results are presented and discussed in Section XI.

The CCM description below does not include effects of wind, since its incorporation is relatively straightforward and will be included in future publications.

II. STOKES FLOW MODEL

Assume that a chaff fiber of length l is longitudinally straight with a circular cross section of radius c, where $c/l \ll 1$. Since the fiber is assumed to descend relatively slowly (~ 0.5 m/s) and is narrow ($c \sim 25 \times 10^{-6}$ m), the Reynolds number Re of the flow about the fiber is small, and the governing (nonlinear) Navier-Stokes equation can be approximated by the (linear) Stokes equation. For Stokes flow, it may be shown that any cylindrically symmetric body that also has a plane of symmetry normal to the cylinder axis will maintain its orientation during constant descent [1]. These symmetry properties are satisfied by the chaff fiber being considered, so that its orientation will be assumed to remain unchanged during descent. In addition to its vertical component, the velocity of the fiber will in general possess a horizontal component as well. Furthermore, by approximating the cylindrical fiber by an elongated spheroid of length l and spheroidal radius c, the vertical and horizontal velocity components v and u may be expressed in closed form as [1]

$$v = \frac{\tilde{v}(\theta)}{\mu(z)} \tag{1}$$

$$\tilde{v}(\theta) = \frac{g\Delta\rho c^2}{6}\left\{\left[\ln\left(\frac{\ell}{c}\right) - \frac{3}{2}\right]\sin^2\theta + \left[\ln\left(\frac{\ell}{c}\right) + \frac{1}{2}\right]\right\}$$

$$u = \frac{g\Delta\rho c^2}{6\mu(z)}\sin\theta\cos\theta\left[\frac{3}{2} - \ln\left(\frac{\ell}{c}\right)\right] \tag{2}$$

where θ is the elevation angle of the fiber (i.e., 0 for horizontal orientation), μ is the atmospheric viscosity which depends on the height z, g is the acceleration due to gravity, and $\Delta\rho = \rho_{\text{body}} - \rho_{\text{air}}$ is the difference in density between the fiber and the air.

The height z_{fiber} of the chaff fiber at any desired time t can be found by using $v = -dz/dt$ in (1) to yield

$$\int_{z_L}^{z_{\text{fiber}}} \mu(z')dz' = -\tilde{v}(\theta)t \tag{3}$$

where it is assumed that the fiber of orientation θ was dispensed at $z = z_L$, $t = 0$ with its equilibrium velocity given by (1) and (2). Equation (3) can in principle be solved for $z_{\text{fiber}}(t,\theta)$.

III. VERTICAL DISTRIBUTION

Now assume that instead of a single fiber with orientation θ, there are many fibers with their orientations characterized by a known probability density distribution $W_\theta(\theta)$. The probability that a given fiber will have an orientation angle less than θ_0 will then be given by

$$P[\theta < \theta_0] = \int_0^{\theta_0} W_\theta(\theta)d\theta. \tag{4}$$

Each fiber would then fall at a velocity given by (1) and be characterized by its value of θ, so that after a time t has elapsed each fiber of the original bundle would be located at a different height z. For this value of time, it is of interest to determine the probability density distribution in height $W_z(z)$, and in horizontal range $W_r(r)$, since these distributions are related to the physical density of the fibers at (r,z,t). $W_r(r)$ will be discussed in Sections V–VIII. In order to determine $W_z(z)$, consider the probability $P[z_{\text{fiber}} > z_a]$ that at a time t any chaff particle chosen at random will be at a height greater than z_a. If the fibers at $z = z_a$ have an elevation angle θ_a, then

$$P[z_{\text{fiber}} > z_a] = P[|\theta| < \theta_a] = \int_0^{\theta_a} W_\theta(\theta)d\theta. \tag{5}$$

Therefore, from the form in (4),

$$W_z(z_a) = -\frac{\partial P[z > z_a]}{\partial z_a} = -\frac{\partial\theta_a(z_a)}{\partial z_a}W_\theta(\theta_a(z_a))$$

$$= \frac{W_\theta(\theta_a(z_a))}{2tu(z_a)}. \tag{6}$$

The last term follows from differentiating (3) with respect to θ and noting from (1) and (2) that

$$\frac{\partial v}{\partial\theta} = -2u. \tag{7}$$

IV. HELICAL MOTION MODEL

The distribution model described thus far would produce a "cloud" of chaff fibers which has properties that are not compatible with experimental data. Examples of such incompatibilities are the following.

1) If the chaff bundle with any orientation distribution $W_\theta(\theta)$ is initially located at $z = z_L$, $r = 0$, then the fibers would form a shell at any later time, rather than the full cloud which has been observed.

2) Since the horizontal velocity u of each fiber is constant in magnitude and direction, then the cloud would constantly expand horizontally in time as it descends, whereas observations have indicated that

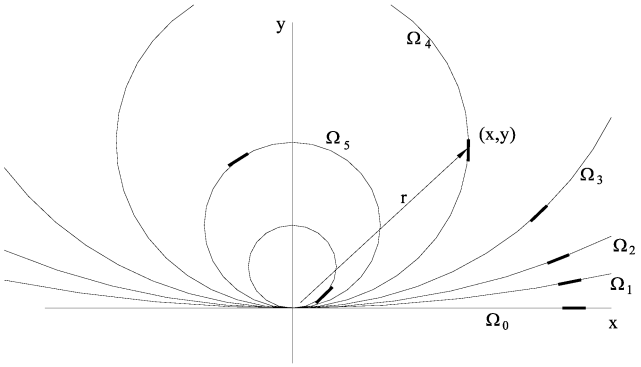

Fig. 1. Location of chaff fibers with same lateral velocity u but different angular velocities Ω_i, after a time t.

a cloud diameter is attained after a finite time beyond which the expansion is negligible.

In a comprehensive laboratory study of the descent of chaff fibers [7], it was observed that their elevation angles did indeed remain constant during fall, and that the direction of the velocity vector during fall is in agreement with (1) and (2). However, it was observed that although the horizontal speed was constant, its direction changes continuously so that its descent is in the form of a helix. This motion was attributed to slight curvatures in the fiber. The probability density distribution $W_\Omega(\Omega)$ of the angular speed Ω was observed in [7] and found to be independent of θ. It is shown below that incorporation of the principle of rotational probability into the chaff model produces results without the incompatibilities listed above.

Consider a conglomerate of identical chaff particles with the same elevation angle θ being dispensed at $z = z_L$, $r = 0$, $t = 0$, but with each fiber having a different rotational velocity characterized by the distribution $W_\Omega(\Omega)$. Further assume for the time being that the initial direction of the horizontal component of the velocity is the same for each fiber (e.g. in the x direction), as is the sense of the rotation (e.g. counter-clockwise). The probability that a given fiber will have a rotational velocity less than Ω_0 is given by

$$P[\Omega < \Omega_0] = \int_0^{\Omega_0} W_\Omega(\Omega) d\Omega \tag{8}$$

where the lower limit of the integral derives from the limitation on the sense of rotation. The projection of the fiber trajectories in the x-y plane, and the projection of the fibers in that plane after a time t has elapsed, are shown in Fig. 1. The movement of all fibers with elevation angle θ would then consist of an ensemble of trajectories similar to those in the figure, but with the initial horizontal velocity spanning all horizontal directions, and both clockwise and counter-clockwise senses. Such an ensemble would yield the expected azimuthal symmetry of the fiber distribution about $r = 0$ (in the absence of wind). For the time being, however, only the situation in Fig. 1 is analyzed.

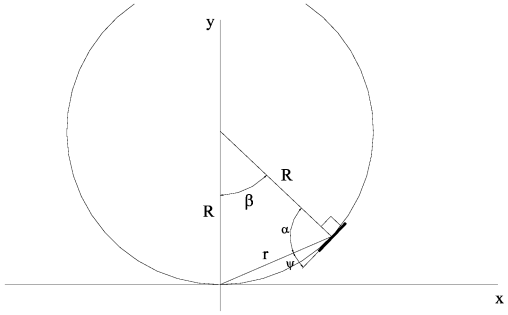

Fig. 2. Geometry for fiber location calculations.

Consider one of the fibers shown in Fig. 1. If its rotational velocity were $\Omega = \Omega_0 = 0$, then the fiber would not circulate, its lateral movement would remain in the x-direction, and after a time t it would have moved a distance ut from its initial position. If, on the other hand, the fiber trajectory corresponds to $\Omega = \Omega_1$, then after a time t it would have moved a distance ut along the trajectory. The radius of the circular trajectory is $R = u/\Omega$, and the angle of the circle traversed in a time t is $\beta = ut/R = \Omega t$. From Fig. 2 the coordinates of the fiber are given by $x = R\sin\beta$, $y = R - R\cos\beta$, so that

$$r = 2R\left|\sin\frac{\beta}{2}\right| = 2\frac{u}{\Omega}\left|\sin\frac{\Omega t}{2}\right|. \tag{9}$$

V. RANGE PROBABILITY

As mentioned previously, the physical density of chaff fibers is related to the probability density $W_r(r)$ of these fibers in any horizontal plane. Referring to Fig. 1, after a time t each fiber will be located at a distance $r(t)$ from $x = y = 0$ given by (9). If the values of Ω in (9) are distributed according to $W_\Omega(\Omega)$, then the corresponding values of $r(t)$ will be distributed according to $W_r(r)$. Although for the case shown in Fig. 1 the values of $r(t)$ correspond to chaff locations in the entire half of the horizontal plane, $W_r(r)$ actually represents a probability density distribution for the entire cloud along any horizontal radial of interest. This can be understood by remembering that the set of trajectories of Fig. 1, for which the initial u is in the x direction, is just one of an ensemble of sets each having a different initial direction for u. Therefore, for every fiber in Fig. 1, there will correspond a fiber of the cloud with the same r, and with an initial u direction that would cause it to coincide with the radial of interest. Since $W_r(r)$ is a linear density with dimensions (length)$^{-1}$/fiber, the horizontal planar density will be given by $W_r(r)/2\pi r$ with dimensions (area)$^{-1}$/fiber. Although this is singular at $r = 0$, it is integrable over the area that includes $r = 0$ after multiplying it by a differential area element.

To determine $W_r(r)$, the probability $P[r < r_0]$ will be found that at a time t a given chaff fiber will be

located at a radial distance r less than some radial distance r_0. This probability will then be expressed in terms of $P[\Omega < \Omega_0]$ which is assumed known. Thus

$$P[r < r_0] = P\left[2\frac{u}{\Omega}\left|\sin\frac{\Omega t}{2}\right| < r_0\right] = P[f(\Phi) < \Gamma] \tag{10}$$

where (9) was used and

$$f(\Phi) = \frac{|\sin\Phi|}{\Phi} \le 1 \tag{11}$$

$$\Gamma = \frac{r_0}{ut}, \qquad \Phi = \frac{\Omega t}{2} \tag{12}$$

and the inequality in (11) follows from the properties of the sinc function. From (10) and (11) it is clear that $f(\Phi) < \Gamma$, $\Gamma > 1$, all Φ, so that

$$P_{\Gamma \ge 1}[r < r_0] = 1 \tag{13}$$

where the subscript on P indicates the values of Γ for which the expression is valid.

If $\Phi_d \equiv 1/\Gamma$, then since the envelope containing the oscillations of $f(\Phi)$ is given by $1/\Phi$, $f(\Phi) < \Gamma$ when $\Phi > 1/\Gamma$, $\Gamma < 1$, or $f(\Phi) < \Gamma$ when $\Phi > \Phi_d$. Therefore, from (10),

$$\begin{aligned} P_{\Gamma<1}[r < r_0] &= P[\Phi > \Phi_d] + P_{\Phi<\Phi_d}[f(\Phi) < \Gamma] \\ &= P[\Phi > \Phi_d] + P[\Phi < \Phi_d] \\ &\quad - P_{\Phi<\Phi_d}[f(\Phi) > \Gamma] \\ &= 1 - P_{\Phi<\Phi_d}[f(\Phi) > \Gamma]. \end{aligned} \tag{14}$$

As discussed in the Appendix, the region $\Phi < \Phi_d$, can be divided into the regions defined by the lobes of $f(\Phi)$. These regions are $\Phi_n < \Phi < \Phi_{n+1}$, where $\Phi_n \equiv n\pi$ and n is an integer $0 \le n \le N$. The last term of (14) will therefore be considered as the sum of the contributions to the probability from each of the lobes of $f(\Phi)$ for $\Phi < \Phi_d$:

$$P_{\Phi<\Phi_d}[f(\Phi) > \Gamma] = \sum_{n=0}^{N} P_{\Phi_n<\Phi<\Phi_{n+1}}[f(\Phi) > \Gamma]. \tag{15}$$

For each term in the sum in (15), the points of intersection between the function $f = f(\Phi)$ and the line $f = \Gamma$ are required. That is, the solutions $\Phi = \Phi_{cn-}$ and $\Phi = \Phi_{cn+}$ are required of (50), where $\Phi_{cn-} < \Phi_{cn+}$. When $n = 0$, only the $\Phi = \Phi_{cn+}$ will be of interest and $\Phi = \Phi_{c0-}$ will be defined as $\Phi_{c0-} \equiv 0$. Equation (15) could then be written

$$\begin{aligned} P_{\Phi<\Phi_d}[f(\Phi) > \Gamma] &= \sum_{n=0}^{N} P[\Phi_{cn-} < \Phi < \Phi_{cn+}] \\ &= \sum_{n=0}^{N} P[2\Phi_{c,n,-}/t < \Omega < 2\Phi_{c,n,+}/t] \end{aligned} \tag{16}$$

where (12) was used. Using (8),

$$\begin{aligned} P_{\Phi<\Phi_d}[f(\Phi) > \Gamma] &= \sum_{n=0}^{N} \int_{2\Phi_{c,n,-}/t}^{2\Phi_{c,n,+}/t} W_\Omega(\Omega)d\Omega \\ &= \frac{2}{t}\sum_{n=0}^{N} \int_{\Phi_{c,n,-}}^{\Phi_{c,n,+}} W_\Omega(2\Phi/t)d\Phi \end{aligned} \tag{17}$$

where (12) was again used to revert back to the Φ variables. This may be written

$$P_{\Phi<\Phi_d}[f(\Phi) > \Gamma] = \frac{2}{t}\int_0^{\Phi_d} F(\Phi)W_\Omega(2\Phi/t)d\Phi \tag{18}$$

where $F(\Phi)$ is zero except within the intervals of integration of (17) where it is unity:

$$F(\Phi) = 1, \Phi_{c,n,-} < \Phi < \Phi_{c,n,+}, \qquad 0 \le n \le N. \tag{19}$$

Using (18) in (14) produces

$$P_{\Gamma<1}[r < r_0] = 1 - \frac{2}{t}\int_0^{\Phi_d} F(\Phi)W_\Omega(2\Phi/t)d\Phi. \tag{20}$$

VI. APPROXIMATE METHODS

It should be emphasized that to this point, no approximations have been implemented in the mathematical derivation of the assumed physical model. Assumptions will now be employed regarding the form of the function $W_\Omega(2\Phi/t)$ which is assumed known. These will utilize statistical observations of $W_\Omega(\Omega)$ which indicate in general that it is maximum for $\Omega = 0$ and decreases to zero at some value Ω_e. Assume now that $W_\Omega(2\Phi/t)$ does not change greatly within each interval of π in Φ. This can be expected to be the case when, if Φ changes by π, the corresponding change in the argument Ω of W_Ω is small relative to the entire Ω domain over which W_Ω is non-zero. That is, if the domain over which $W_\Omega(\Omega)$ is non-zero extends from 0 to Ω_e, then $W_\Omega(2\Phi/t)$ will not change greatly within each interval of π in Φ if $2\pi/t \ll \Omega_e$, or $t \gg 2\pi/\Omega_e$. In such a case, a typical interval over π of the integral in (20) can be written

$$\begin{aligned} &\int_{\Phi_n}^{\Phi_n+\pi} F(\Phi)W_\Omega(2\Phi/t)d\Phi \\ &\quad \approx W_\Omega(\Omega_n)[\Phi_{c,n,+} - \Phi_{c,n,-}] \\ &\quad = W_\Omega(2\Phi_n/t)F(\Phi_n + \pi/2)[(\Phi_n + \pi) - \Phi_n] \\ &\quad \approx \int_{\Phi_n}^{\Phi_n+\pi} W_\Omega(2\Phi_n/t)F(\Phi)d\Phi \end{aligned} \tag{21}$$

where now

$$F(\Phi) \approx \frac{\Phi_{c,n,+} - \Phi_{c,n,-}}{\pi}$$

$$\Phi_n < \Phi < \Phi_n + \pi, \qquad 0 \le n \le N \tag{22}$$

is defined over the entire interval rather than over a portion of the interval, and is the fraction of the interval of integration relative to π.

In the Appendix, it is shown that the Φ_{cn+}, Φ_{cn-} are roots of (50). Since the last term of $t(\phi)$ in (51) is $(n+1/2)\Gamma\pi = \Phi_{n+1/2}/\Phi_d$, the Φ_{cn+} and Φ_{cn-} will be functions of $\Phi_{n+1/2}/\Phi_d$. If now it is desired to approximate the discrete values of $F(\Phi)$ in each interval as a continuous function defined over the entire interval of integration, this can be accomplished by expressing the $\Phi_{n+1/2}/\Phi_d$ as Φ/Φ_d. Therefore, $F(\Phi)$ can be written

$$F(\Phi) = G\left(\frac{\Phi}{\Phi_d}\right). \tag{23}$$

Substituting (23) into (20), yields

$$P_{\Gamma<1}[r<r_0] = 1 - \frac{2u}{r_0}\int_0^1 G(\lambda)W_\Omega(2\lambda u/r_0)d\lambda \tag{24}$$

where $\lambda = \Phi/\Phi_d = \Phi r_0/(ut)$. Performing the integration by parts yields

$$P_{\Gamma<1}[r<r_0] = 1 - 2\frac{u}{r_0}\left\{W_\Omega\left(\frac{2u}{r_0}\right)H(1) - W_\Omega(0)H(0)]\right\} + 2\frac{u}{r_0}\int_0^1 \frac{dW_\Omega\left(\frac{2\lambda u}{r_0}\right)}{d\lambda}H(\lambda)d\lambda \tag{25}$$

where $H(\lambda) = \int G(\lambda)d\lambda$.

VII. CLOSED FORM SOLUTION

The known probability density $W_\Omega(\Omega)$ can be numerically approximated to any desired degree of accuracy in terms of a piecewise linear function. Based on the experimental observations of [7], $W_\Omega(\Omega)$ will be approximated as linear in the region over which it is non-zero:

$$W_\Omega(\Omega) = \frac{2}{\Omega_e}\left(1 - \frac{\Omega}{\Omega_e}\right), \qquad 0<\Omega<\Omega_e \tag{26}$$

which is normalized so that $\int_0^{\Omega_f} W_\Omega(\Omega)d\Omega = 1$ for $\Omega_f > \Omega_e$. Defining $\Phi_e = \Omega_e t/2$, $\lambda_e = \Phi_e/\Phi_d = \Omega_e r_0/(2u)$, (26) may be written

$$W_\Omega(2\lambda u/r_0) = \frac{2}{\Omega_e}\left(1 - \frac{\lambda}{\lambda_e}\right), \qquad 0<\lambda<\lambda_e. \tag{27}$$

Using (27), the integral in (25) may be evaluated as

$$\int_0^1 \frac{dW_\Omega\left(\frac{2\lambda u}{r_0}\right)}{d\lambda}H(\lambda)d\lambda = -\frac{2}{\Omega_e\lambda_e}\int_0^{\lambda_e} H(\lambda)d\lambda = -\frac{4u}{\Omega_e^2 r_0}[I(\lambda_e) - I(0)] \tag{28}$$

TABLE I
Integrals of Candidate $G(\lambda)$ Function

$G(\lambda)$	$(2/\pi)\cos^{-1}\lambda$
$H(\lambda)$	$(2/\pi)[\lambda\cos^{-1}\lambda - (1-\lambda^2)^{1/2}]$
$I(\lambda)$	$(2/\pi)[(\lambda^2/2 - 1/4)\cos^{-1}\lambda - (3\lambda/4)(1-\lambda^2)^{1/2} - (1/2)\sin^{-1}\lambda]$
$H(0)$	$-2/\pi$
$H(1)$	0
$I(0)$	$-1/4$
$I(1)$	$-1/2$

where $I(\lambda) = \int H(\lambda)d\lambda$. In (28), if $1 < \lambda_e$, then 1 is used in place of λ_e. Using (27) and (28), (25) becomes

$$P_{\Gamma<1}[r<r_0] = 1 - 2\mu[(1-\mu)H(1) - H(0)] - 2\mu^2[I(1/\mu) - I(0)] \tag{29}$$

where $\mu = (2u/r_0\Omega_e) = (1/\lambda_e) = (1/\Gamma\Phi_e) = (\Phi_d/\Phi_e)$.

When $\lambda_e > 1$, then $\mu < 1$ and $\Gamma > 1/\Phi_e$. Equation (29) then becomes

$$P_{\Gamma<1}[r<r_0] = 1 - 2\mu\{H(1) - H(0) + \mu[I(1) - I(0) - H(1)]\}, \qquad \mu<1. \tag{30}$$

In the limit of $r_0 \to \infty$, $\mu \to 0$ so that $P_{\Gamma<1}[r<r_0] \to 1$ as would be expected. When $\lambda_e < 1$, then $\mu > 1$ and $\Gamma > 1/\Phi_e$, and (29) may be written

$$P_{\Gamma<1}[r<r_0] = 1 + 2\frac{\lambda_e H(0) - [I(\lambda_e) - I(0)]}{\lambda_e^2}, \qquad \lambda_e<1. \tag{31}$$

In the limit $\lambda_e \to 0$, the right hand term is indeterminate, but may be evaluated using the L'Hospital rule twice, leading to $P_{\Gamma<1}[r<r_0] = \lim_{\lambda_e\to 0} 1 - G(0)$. Now it is clear that $P[r<r_0] \to 0$ as $r_0 \to 0$. Also, from (22) and (23) it may be seen that near $\Phi = \Phi_d$ or $\lambda = 1$, $\Phi_{c,n,+} - \Phi_{c,n,-} \to 0$. Therefore, two requirements on the function $G(\lambda)$ are

$$G(0) = 1, \qquad G(1) = 0. \tag{32}$$

The precise expression for G would depend on the approximation used to obtain the roots of (50). If each lobe of the function $f(\Phi)$ is approximated as a sin function, then $G(\lambda)$ may be obtained from (54), and satisfies (32). It and its integrals are shown in Table I.

The approximation of $G(\lambda)$ shown in Table I is not valid for the integration over the $n = 0$ term in (15). Although this term may be separated from the rest of the sum, the formal results given by (30) and (31) will be used unless Γ is such that $n = 0$ is the only term in the sum of (15). This will occur when $N = 0$ in (22), and corresponds to $\Gamma_0 < \Gamma < 1$, where $\Gamma_0 = 0.2172336$. For this case it may be shown that

$$P_{\Gamma<1}[r<r_0] = \left[1 - \frac{\min(\Phi_{c0+}, \Phi_e)}{\Phi_e}\right]^2, \qquad N = 0. \tag{33}$$

VIII. PROBABILITY DENSITY

The probability density $W_r(r_0)$ is 0 except when $\Gamma < 1$:

$$W_r(r_0) = \frac{\partial P_{\Gamma<1}[r < r_0]}{\partial r_0}, \qquad \Gamma < 1. \tag{34}$$

Applying this to (30), and noting that the only r_0 dependence enters through the parameter μ,

$$W_r(r_0) = -\frac{2\mu}{r_0}\{H(0) - H(1) + 2\mu[I(0) - I(1) + H(1)]\}, \qquad \mu < 1 \tag{35}$$

where $(\partial\mu/\partial r_0) = -(\Omega_e/2u)\mu^2 = -(\mu/r_0)$ was used. Applying (34) to (31) yields

$$W_r(r_0) = -\frac{\Omega_e}{u}\mu^2\{H(0) + H(1/\mu) + 2\mu[I(0) - I(1/\mu)]\}, \qquad \mu > 1. \tag{36}$$

Applying the L'hospital formula to (36) and employing Table I, the limit as $\mu \to \infty$ can be written

$$W_r(0) = W_r(r_0)_{\lim\lambda_e \to 0} = -\frac{\Omega_e}{6u}G'(\lambda_e) = \frac{\Omega_e}{3\pi u}. \tag{37}$$

IX. CHAFF CLOUD SIZE

From the foregoing discussion, there will always be chaff particles with angular velocity $\Omega = 0$ or close to it, implying the outer edge of the chaff cloud will continually distant itself from the cloud center at a velocity u. The radius of the cloud will therefore be

$$r_{0c} = ut \tag{38}$$

on which $\Gamma = 1$. However, since only a relatively small fraction of fibers will be located near the cloud edge, this ever-expanding edge does not necessarily provide a useful characterization of the cloud size. It is often more useful to characterize the size of the chaff cloud by the region about the center that contains a certain fraction of the total particles, say $p_0 = 0.9$ or 0.95. This information can be provided by inverting the probability function $p_0(\mu) = P[r < r_0]$ to obtain the values of r_0 as a function of p_0.

Since $p_0(\mu)$ is a monotonically increasing function of r_0, it is a monotonically decreasing function of μ. Also, from (29) and (30), $p_0(1) = 0.2267$ when $\mu = 1$. Therefore, when $p_0(\mu) > p_0(1)$, $\mu < 1$, and the equation for $p_0(\mu)$ is given by (30) which can be written

$$\alpha\mu^2 + 2\beta\mu + \gamma = 0, \qquad \Gamma < 1 \tag{39}$$

where

$$\alpha = 2[I(1) - I(0) - H(1)], \qquad \beta = H(1) - H(0), \qquad \gamma = p_0 - 1. \tag{40}$$

Solving (39) yields

$$\mu = \frac{2}{\Gamma\Omega_e t} = \frac{2u}{r_0\Omega_e} = \frac{-\beta + \sqrt{\beta^2 - \alpha\gamma}}{\alpha}, \qquad \Gamma < 1 \tag{41}$$

where the branch of the solution was chosen to assure $\mu \to 0$ as $p_0 \to 1$ in accordance with the discussion following (30) and using the fact that $\beta > 0$. Solving for the desired value of r_0 and using (40) and Table I yields

$$r_0 = r_{0c} = \frac{2u\alpha}{\Omega_e\left(-\beta + \sqrt{\beta^2 - \alpha\gamma}\right)} \approx \frac{8u}{\Omega_e\pi|\gamma|} < ut \tag{42}$$

which assumed $|\gamma| \ll 1$ that is consistent with $p_0 > p_0(1)$, and the inequality expresses the condition $\Gamma < 1$ for (42) to be valid. Equations (38) and (42) can be combined to yield

$$r_{0c} \approx \min\left(ut, \frac{8u}{\Omega_e\pi|\gamma|}\right). \tag{43}$$

X. FIBER ORIENTATION AND RCS

For purposes of RCS computation, it is customary to consider the chaff fiber as a conducting finite circular cylinder with length far exceeding its cross sectional radius [4–6]. If the angle between the incident wave direction and the fiber axis is ξ, then the monostatic RCS may be written

$$\sigma(\xi) = \frac{\lambda^2}{\pi}|S(\xi)|^2$$

where λ is the wave length. $S(\xi)$ is related to the scattered electric field E_ξ^s through

$$E_\xi^s(r, \xi) = \frac{e^{ikr}}{kr}S(\xi)$$

where $k = 2\pi/\lambda$ is the wave number and r is the radial coordinate with origin at the center of the fiber. The ξ subscript on E indicates that the scattered electric field vector lies in the plane of the fiber and the incident wave direction.

Methods to determine $S(\xi)$, and consequently $\sigma(\xi)$, are readily available [2, 3]. In addition to ξ, the value of $\sigma(\xi)$ will depend on the radiation frequency, the fiber length and radius, and the component of the incident electric field parallel to the fiber (i.e. the polarization). The latter, like ξ, is a function of the fiber orientation. Although the elevation angle of each fiber relative to the horizontal is assumed known (and would have been used to obtain the lateral velocity u), its azimuthal orientation, or orientation of its projection onto the x-y plane, must now be addressed. This is characterized by the angle ψ in Fig. 2 between the projection and the radial to the fiber.

Consider the chaff cloud after a time t has elapsed. For any particular value r_e of r_0, there will be a finite number of circular trajectories of Fig. 1 for which a chaff fiber is located at a distance r_e from $x = y = 0$. Consider one such fiber, say fiber a, that moves along trajectory Ω_a. Since the time t and the radial distance r_e define a value for Γ, the angular velocity Ω_a is a solution to (9) at $r = r_e$. From Fig. 2, $\beta_a = \Omega_a t = 2\Phi_a$, and the angle $\psi = \psi_a$ is given by

$$\psi_a = \frac{\pi}{2} - \alpha_a = \frac{\pi}{2} - \frac{\pi - \beta_a}{2} = \frac{\beta_a}{2} = \mathrm{mod}(\Phi_a, \pi). \tag{44}$$

Similar expressions would be obtained for all other fibers that are a distance r_e from the origin. The number of such fibers will correspond to the number of solutions to (9), namely $2N + 1$. The horizontal projection of each one of these fibers will be oriented at a different angle ψ relative to the radial to it.

Although the above result applies to chaff fibers at different locations in the half plane shown in Fig. 1, it can be extended to the entire cloud by applying the previously discussed principle that the full cloud is composed of an ensemble of trajectory sets with initial horizontal velocity u in all directions. Therefore, at a time t, there will be $N_f = 2(2N + 1)$ fibers at each point along any circumference $r = r_e$ each characterized by the different values of $\psi = \psi_n$, $1 \le n \le N_f$ as discussed above. The factor of 2 above follows from the fact that the ensemble includes both clockwise and counter-clockwise movements, with the values of ψ for the clockwise sense being symmetric to those for the counter-clockwise sense relative to the radial of interest.

The backscatter RCS of the nth fiber in any given direction may be denoted $\sigma_{n\{h\ v\}}(r_e, \varphi, \psi_n, \theta)$, where the polarization is indicated by h (horizontal) or v (vertical), and φ represents the azimuthal location of the fiber of interest in the horizontal plane. The average RCS of a chaff particle over all chaff particles at this location will be given by

$$\sigma_{\mathrm{avg}\{h\ v\}}(r_e, \varphi) = \frac{\sum_{n=1}^{N_f} \sigma_{n\{h\ v\}}(r_e, \varphi, \psi_n, \theta)}{N_f}. \tag{45}$$

This assumes that the RCS of many fibers is the sum of the RCS of the individual fibers. This has been shown to be the case for a large number of fibers separated from each other by a distance that is large relative to a wave length, and when their locations are random over a distance of a wave length [9]. These conditions can be assumed to already hold at times that are small relative to times of usual interest in chaff problems.

In situations in which computations of (45) are to be combined with real time radar simulations, the computation time required to evaluate that sum can become prohibitive when $N_f \gg 1$. It was found in such cases that a judicious method of sampling these directions will lead to excellent results using a relatively small number of terms in the sum.

Recall now that $W_r(r)/2\pi r$ and $W_z(z)$ are normalized densities in the horizontal plane and in the vertical direction, respectively. If N_{tot} is the total number of chaff particles present, then the number of chaff particles within the differential volume $r\,dr\,dz\,d\varphi$ will be given by $= N_{\mathrm{tot}}(W_r(r)/2\pi r)W_z(z)r\,dr\,dz\,d\varphi$. The total RCS due to particles in the differential volume $r\,dr\,dz\,d\varphi$ will then be

$$\begin{aligned}\sigma_{\{h\ v\}}(r, \varphi, z) &= N_{d\mathrm{vol}}(r)\sigma_{\{h\ v\}\mathrm{avg}}(r, \varphi) \\ &= N_{\mathrm{tot}}\sigma_{\{h\ v\}\mathrm{avg}}(r, \varphi)\frac{W_r(r)}{2\pi r}W_z(z)r\,dr\,dz\,d\varphi.\end{aligned} \tag{46}$$

The normalized RCS density at the differential volume is therefore

$$\begin{aligned}\eta_{\{h\ v\}}(r, \varphi, z) &= \frac{\sigma_{\{h\ v\}}(r, \varphi, z)}{N_{\mathrm{tot}}r\,dr\,dz\,d\varphi} \\ &= \sigma_{\{h\ v\}\mathrm{avg}}(r, \varphi)\frac{W_r(r)}{2\pi r}W_z(z).\end{aligned} \tag{47}$$

In practical radar problems, it is desired to determine the chaff RCS within a finite volume defined by the radar beamwidth and the range cell size. If in such a case the vertical extent of the volume is from z_i to z_f, then the RCS $\sigma_{\mathrm{tot}\{h\ v\}}(r, \varphi, z)$ within the finite volume will be given as the integral over (47), with the integral over z being evaluated immediately:

$$\begin{aligned}&\sigma_{\mathrm{tot}\{h\ v\}}(r, \varphi, z) \\ &= N_{\mathrm{tot}}(P[z < z_f] - P[z < z_i])\int\int \sigma_{\{h\ v\}\mathrm{avg}}(r, \varphi)\frac{W_r(r)}{2\pi r}r\,dr\,d\varphi.\end{aligned} \tag{48}$$

XI. RESULTS AND DISCUSSION

Using the theory and methods described above, the following procedure would be used to determine the RCS density at the time t and at the point (r, φ, z) within the cloud, assuming $W_\theta(\theta)$ and $W_\Omega(\Omega)$ (or Ω_e in (26)) are known.

1) Find the tilt elevation angle θ from (3).
2) Find the probability density $W_z(z)$ using $W_\theta(\theta)$ in (6).
3) Find the lateral velocity u from (2).
4) Find $W_r(r_0)$ from (35) or (36).
5) Find the azimuthal fiber orientations ψ_i from (44).
6) Find the average RCS at the point from (45).
7) Find the normalized RCS density from (47).

This procedure assumes that at $t = 0$, all the fibers are concentrated at the point $z = z_L$, $r_0 = 0$, and each of the fibers is moving at its equilibrium velocity corresponding to its orientation angle θ. The validity of these assumptions is based on observed rapid

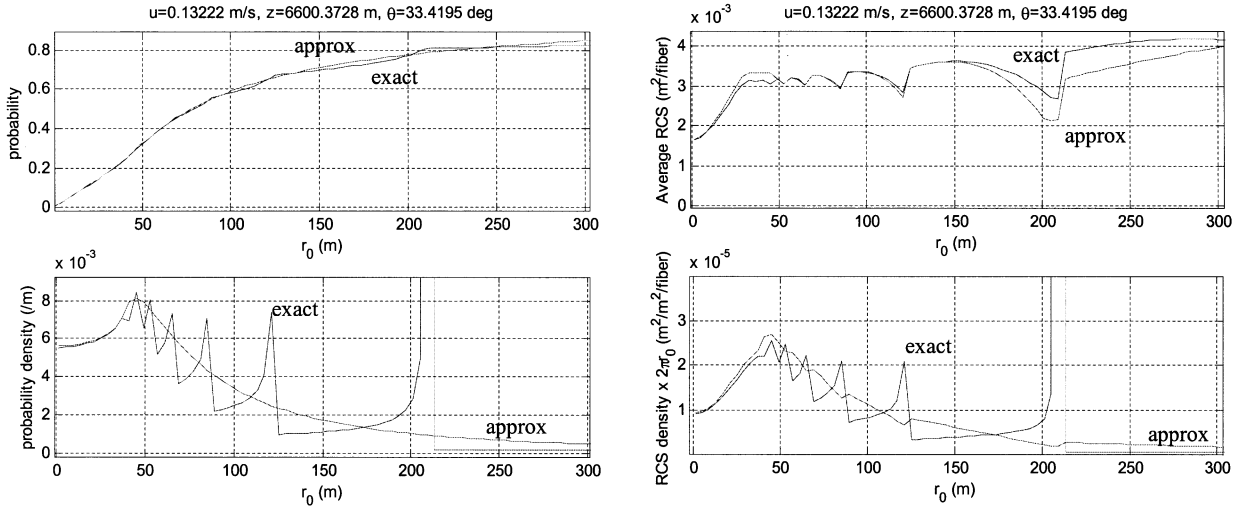

Fig. 3. Cloud parameters as function of radial distance.

transitions to equilibrium [7], so that any temporal or spatial discrepancies can be ignored relative to the times and distances of interest.

Consider fibers 1 mil in diameter that are tuned to 2.3 GHz and are dispensed at a height of 10 km. The viscosity μ is assumed to vary linearly with height as an approximation to the ARDC Model Atmosphere [10]. The approximation $\Omega_e \approx 0.007$ rad/s is obtained from (42) as that value required to produce a maximum cloud radius of 725 m when $u = 0.2$ and $p_0 = 0.9$. In accordance with reports that most fibers tend to be oriented near the horizontal [4, 5], the probability density distribution for orientation will be taken as zero except within the region $0 < \theta < \theta_e$, where

$$W_\theta(\theta) = \frac{2}{\theta_e}\left(1 - \frac{\theta}{\theta_e}\right), \qquad 0 < \theta < \theta_e \tag{49}$$

and θ_e is taken as 40°. At a time 120 min after the chaff is dispensed, the cloud would have a vertical extent from 6.4 to 7.2 kms in altitude. At the height of 6.6 kms, the lateral fiber speed would be $u =$ 0.132 m/s. Using the model described herein, Fig. 3 provides exact and approximate results for $P(r < r_0)$, $W_r(r_0)$, $\sigma_{h,\text{avg}}(r_0, 45°)$, $\eta_h(r_0, 45°, z)$ as a function of r_0. The h subscript indicates that the RCS results refer to horizontal polarization. The radar is assumed to be at the same height as the cloud. The exact results are obtained using (17) (and were independently verified by comparing them with results obtained using a Monte Carlo scheme), while the approximate results are obtained using (30) and (31) with Table I. For RCS computations, the approximate results also include replacing the numerator on the right of (45) by a sum over a small number of orientations judiciously chosen to characterize the original sum. Only the inner third of the cloud is shown, since the behavior of the cloud beyond the range shown does not change appreciably and its contribution to the RCS density is small.

The exact and approximate results for $W_r(r_0)$ agree well for small values of r_0, and satisfy (37) at $r_0 = 0$. The most obvious difference between the exact and approximate results relates to the spikes in the exact $W_r(r_0)$ function for larger values of r_0. Since there appears to be excellent agreement for $P(r < r_0)$, and since $W_r(r_0)$ is its derivative, the spikes can be traced to relatively rapid changes in the derivative of $P(r < r_0)$ at the "spike" points which are at values of r_0 across which the number of terms N changes in the sum of (17). This is immediately apparent from the exact solution in (14) since $P(r < r_0)$ behaves differently according to whether $f(\Phi) > \Gamma$ or $f(\Phi) < \Gamma$. The approximation to $P(r < r_0)$, on the other hand, smoothes over these functional differences and therefore no spikes of its derivative are observed. Now the physical source of the spikes can be traced to the well-defined characteristics of the fiber movement in the proposed model. Since these assumptions are themselves approximations, it would be unlikely that such "singular" behavior as the spikes that appear in Fig. 3 would appear in reality. In this sense, then, the smoothed approximations can be expected to be more reliable than the exact solution.

The approximations of the normalized RCS densities $\eta_h(r, 45°, z)$ and $\eta_v(r, 45°, z)$ in a vertical plane at an angle 45° to the radar direction are shown in Fig. 4. These were obtained from (47) in which the approximate solution for $W_r(r)$ was used. Since the fibers are weighted heavily toward horizontal orientation in accordance with (49), the horizontally polarized RCS is seen to greatly exceed that for vertical polarization. Also, since the horizontally oriented fibers fall more slowly, the horizontally polarized contribution is strongest at the highest altitude in agreement with observations [8]. For vertical polarization, the RCS density is more uniform with altitude since the fiber density decreases with

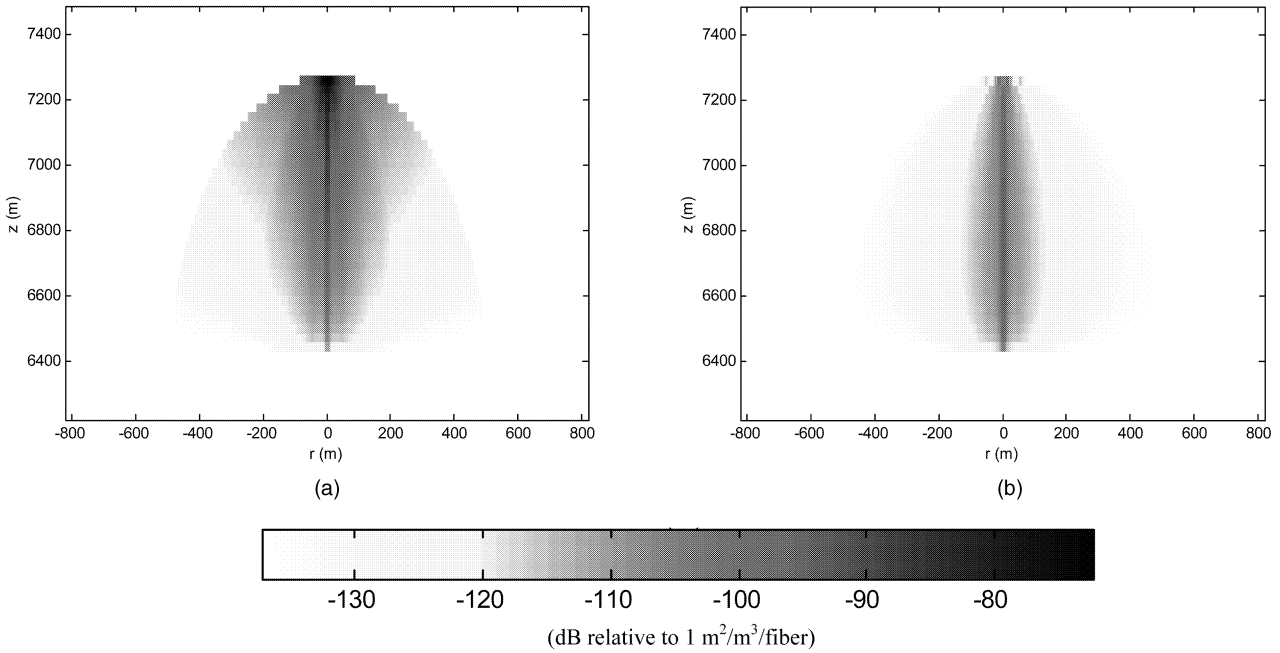

Fig. 4. Gray scale maps of RCS density for (a) horizontal and (b) vertical polarizations.

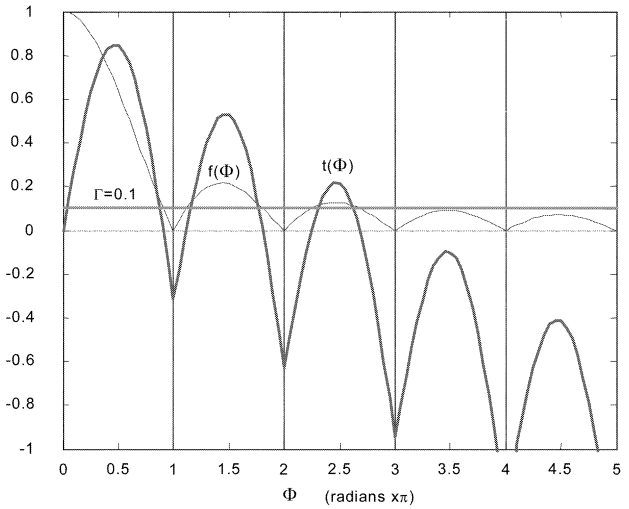

Fig. 5. Functions related to $\sin\Phi/\Phi = \Gamma$.

decreasing altitude while the fiber orientation becomes more vertical with decreasing altitude.

APPENDIX. PROPERTIES OF $f(\Phi) = \Gamma$

Consider the equation $f(\Phi) = \Gamma$ where $f(\Phi) = |\sin\Phi|/\Phi$ and Γ is a positive constant < 1. This can be rewritten

$$t(\Phi) = |\sin\Phi| - \Gamma\,\Phi = 0 \tag{50}$$

which, by substituting $\Phi = (n + 1/2)\pi + \phi$, $\Phi_n < \Phi < \Phi_{n+1}$, $\Phi_n \equiv n\pi$, into (50) would yield

$$t(\phi) = \cos\phi - \Gamma\,\phi - (n + 1/2)\Gamma\,\pi, \qquad -\pi/2 < \phi < \pi/2. \tag{51}$$

The functions $f(\Phi)$, and $t(\Phi)$ with $\Gamma = 0.1$, are shown in Fig. 5.

It is clear from the figure that when solutions exist, they appear in pairs within each region $\Phi_n < \Phi < \Phi_{n+1}$, $n > 0$. For $0 < \Phi < \pi$, there would only be a single solution. Referring to these solutions as Φ_{cn-} and Φ_{cn+}, they may be obtained within each region to any desired degree of accuracy using an appropriate iterative scheme. Approximations for these functions may be obtained by approximating each lobe of $f(\Phi)$ as a simple function such as

$$\frac{|\sin\Phi|}{\Phi} \approx \begin{cases} \cos(\Phi/2), & \\ & \Phi_n < \Phi < \Phi_{n+1}, \quad n = 0, \\ \dfrac{1}{\Phi_n + \pi/2}\cos[\Phi - (\Phi_n + \pi/2)], & \\ & \Phi_n < \Phi < \Phi_{n+1}, \quad n > 0. \end{cases} \tag{52}$$

Substituting (A3) into (A1) leads to the solutions

$$\Phi_{cn\pm} \approx \begin{cases} 2\cos^{-1}\Gamma, & \\ & \Phi_n < \Phi < \Phi_{n+1}, \quad n = 0, \\ \Phi_n + \pi/2 \pm \cos^{-1}[(\Phi_n + \pi/2)\Gamma], & \\ & \Phi_n < \Phi < \Phi_{n+1}, \quad 1 \le n \le N. \end{cases} \tag{53}$$

From (22) and (23),

$$G(\lambda) \approx \begin{cases} (2/\pi)\cos^{-1}\Gamma, & 0 < \lambda < \Phi_1/\Phi_d, \\ (2/\pi)\cos^{-1}\lambda, & \Phi_1/\Phi_d < \lambda < 1. \end{cases} \tag{54}$$

The solutions in (53) may be improved greatly by using the first Newton-Raphson correction.

ACKNOWLEDGMENT

The author wishes to thank Elad Tomer, Zvi Penner, and Dennis Mihora for many useful discussions and ideas.

REFERENCES

[1] Happel, J., and Brenner, H. (1973)
Low Reynolds Number Hydrodynamics.
Leyden, Netherlands: Noordhoff, 1973.

[2] Van Vleck, J. H., Bloch, F., and Hamermesh, M. (1947)
Theory of radar reflections from wires or thin metallic strips.
Journal of Appllied Physics, **18** (1947), 274–294.

[3] Einarsson, O. (1987)
The wire.
In J. J. Bowman, T. B. A. Senior, and P. L. E. Uslenghi, Eds., *Electromagnetic and Acoustic Scattering by Simple Shapes*, New York: Hemisphere, 1987, 472–502.

[4] Palermo, C. J., and Bauer, L. H. (1965)
Bistatic scattering cross section of chaff dipoles with application to communications.
Proceedings of the IEEE, **53**, 8 (Aug. 1965), 1119–1121.

[5] Butters, B. C. F. (1982)
Chaff.
IEE Proceedings Pt. F, **129**, 3 (June 1982), 197–201.

[6] Guo, Y., and Uberall, H. (1992)
Bistatic radar scattering by a chaff cloud.
IEEE Transactions on Antennas Propagation, **40**, 7 (July 1992), 837–841.

[7] Brunk, J., Mihora, D., and Jaffe, P. (1975)
Chaff aerodynamics.
Report AFAL-TR-75-81, Nov. 1975.

[8] van Brunt, L. B. (1978)
Applied ECM, Vol. 1.
EW Engineering, Dunn Loring, VA, 1978.

[9] Wickliff, R. G., and Garbacz, R. J. (1974)
The average backscattering cross section of clouds of randomized resonant dipoles.
IEEE Transactions on Antennas Propagation, **AP-22**, 3 (May 1974), 503–506.

[10] U.S. Air Force (1961)
Handbook of Geophysics.
New York: MacMillan, 1961.

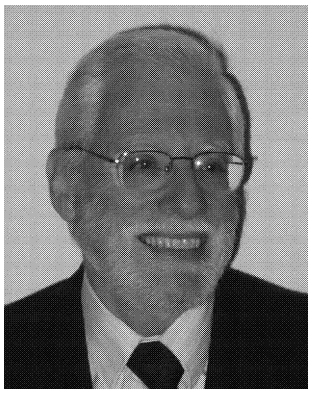

Sherman Marcus (M'80—SM'89) received the B.A. and M.A. degrees in physics from Yeshiva University in 1963 and 1965, respectively, and the Ph.D. degree in applied physics from the Catholic University of America in 1972.

As a physicist for the U.S. Naval Ship Engineering Center from 1967 to 1973, he was active in the investigation of nuclear weapons effects on ships. From 1973 to 1979, and from 1980 to the present, he has been on the research staff of RAFAEL. From 1979 to 1980 he was a research engineer at IIT Research Institute in Annapolis, MD, where he continued to provide consulting services until 1990. From 1992 to 1998 he was also an adjunct senior teaching associate at the Technion, Israel Institute of Technology. During these periods, he was engaged in the development of analytical and numerical methods for predicting propagation and scattering of electromagnetic and acoustic waves, with emphasis on the effects of duct environments and on development and use of parallelization algorithms. His current area of interest is computer simulation of modern radars and electronic countermeasures.

Dr. Marcus has published many journal articles, and has presented papers and lectured at numerous professional conferences.